AIAA 2001-2789

General Asymptotic Solutions for the Oscillatory Channel Flow with Arbitrary Suction

Todd A. Jankowski and Joseph Majdalani
Marquette University
Milwaukee, WI 53233

31st AIAA Fluid Dynamics Conference
11–14 June 2001
Anaheim, CA

General Asymptotic Solutions for the Oscillatory Channel Flow with Arbitrary Suction

T. A. Jankowski* and J. Majdalani†
Marquette University, Milwaukee, WI 53233

This paper considers a porous channel in which a suction-driven flow is present due to arbitrary levels of fluid extraction along the lateral walls. When small amplitude oscillations are introduced, a rotational wave motion is established that this study attempts to analyze. For an elongated channel, two asymptotic methods are used to solve the resulting convection-diffusion equation. The first technique is based on a two-variable multiple-scales expansion that takes into account the thin boundary layer near the wall. While retaining generality of expression, the multiple-scales procedure is carried out until a closed-form solution for the velocity field is obtained for an arbitrary mean-flow function *F*. An alternative approach based on WKB exponentials is also employed. The latter yields two wave solutions traveling in opposite directions. After demonstrating the illegitimacy of the wave traveling into the solid wall, a uniformly valid WKB expansion is obtained. Due to a transcendental integral arising in the WKB expression, only a quasi-closed WKB solution is realized for arbitrary *F*. Both asymptotic formulations agree with one another and with numeric simulations of the problem. They also agree with limiting process solutions that exist for small or large suction levels.

I. Introduction

THE fate of shear layers in well-established flows remains a central topic in fluid mechanics despite the considerable attention that it has received in the past. Almost every conceivable prototypical flow has undergone much scrutiny in this manner, including channel flows with porous walls. In fact, a number of boundary layer studies have been undertaken in the context of better understanding the multiple solutions of Berman's equation with wall suction or injection.[1] Examples abound in the literature and, for a thorough investigation of solution attributes that accompany suction-driven flows, the reader is referred to the survey by Zaturska, Drazin and Banks.[2] For multi-dimensional considerations, one may also be interested in the work of Cox[3] and Taylor, Banks, Zaturska and Drazin.[4] For injection-driven flows, one may find useful the time-dependent analyses and references found in Majdalani.[5]

In the latter work, harmonic pressure disturbances were superimposed on the injection-driven field in a porous channel. The resulting oscillatory motion was found to exhibit rich vortical patterns with relatively large depths of penetration and near-wall velocity overshoot. The problem was also found to exhibit a nonlinear scaling structure due to the co-existence of several physical mechanisms within a sandwiched boundary layer. Although paradoxical at first glance, increasing viscosity led to faster vortical attenuation and reduction in the rotational depth of penetration. Furthermore, the traditionally thin viscous layer was blown off the wall to some intermediate position that could not be localized. Under those circumstances, the penetration depth denoted the rotational region extending from the wall to the location of the shear layer. Obtaining asymptotic solutions required a careful application of multiple-scale and WKB theories over different ranges of the crossflow Reynolds number R.

The main purpose of this article is to complete our oscillatory flow study by extending Majdalani's work[5] to suction-driven fluids. Despite the similarity of the governing equations with the injection-flow analogue,[5] it will be shown that the presence of suction significantly alters the flow character. This is due to several reasons. As remarked by Catheral,[6] the viscous shear layer in injection-driven flows is pushed a distance from the wall in a manner to delineate two regions of virtually inviscid flow: the first is the axial main stream, and the second consists of the sidewall influx. According to Proudman[7] or Cole and Aroesty,[8]

*Graduate Student and Research Associate. Member AIAA.

†Assistant Professor, Department of Mechanical and Industrial Engineering. Member AIAA.

an added difficulty can be expected due to the inability to predict the position of the viscous layer. Our knowledge appears to be limited, as pointed out by Terrill,[9] to the expectation that the layer of order $|R|^{-½}$ will draw nearer to the core with successive increases in injection. Moreover, the nonlinear scaling composition cannot be predicted by conventional transformations that rely on linear distortions of the independent coordinate.

In the presence of suction, however, the salient mean-flow features change in character. Streamlines switch direction as the flow heads to the closed end before undergoing withdrawal at the porous boundaries. Instead of being blown-off the wall, a distinct shear layer is now formed directly above the porous surface. The resulting boundary layer is consistent with Prandtl's usage of the term and increases in size with viscosity (cf. Proudman[7]). It also coincides with the rotational depth of penetration that accompanies steady and periodic flows over hard walls. Unlike the injection-induced penetration depth that increases at higher injection, the suction-induced layer diminishes as suction is increased. By virtue of these mean-flow differences, one expects dissimilarities in the oscillatory wave motion and its underlying scaling structure. A separate mathematical treatment is clearly necessary to solve the resulting boundary value problem. In that spirit, the forthcoming analysis is hoped to provide the formalism needed to obtain uniformly valid approximations for the oscillatory suction-driven channel flow.

Suction-induced flows were first analyzed by Taylor[10] in a manufacturing process that involved running watery suspensions of fibers over porous sheets through which the fluid could be drained to form paper. Other applications have risen in the modeling of isotope separation,[1] irrigation systems,[11] sweat cooling,[12,13] boundary layer control,[14] and other filtration mechanisms. They have also been important in the modeling of the respiratory function in the lungs.[15]

Since past studies have focused on steady flow conditions, this work attempts to account for small amplitude oscillations that are often introduced by inevitable fluctuations in the suction rate itself. In other occasions, the periodic motion is externally induced by moving boundaries such as those considered in the modeling of the respiratory and circulatory functions in biological organisms. Regardless of the source of periodicity, this study seeks approximate solutions for the oscillatory field in the presence of arbitrary wall suction.

The analysis begins in Sec. II with a description of the physical geometry and system constraints. In Sec. III, the governing equations are presented in their general dimensional form. Subsequently, equations and variables are normalized, linearized and decomposed into steady and time-dependent sets. The temporal field is further decomposed using the momentum transport formulation. In Sec. IV, the multiple-scales approach is applied using two linear coordinate transformations. Next, the WKB approach is applied in Sec V. A discussion is presented in Sec VI in which comparisons with numerics are reported. Limiting process verifications are also provided. Finally, concluding remarks are given in Sec. VII.

II. The Basic Flow Model

A. The Porous Channel

A long low aspect ratio channel is modeled with porous top and bottom surfaces separated by a distance $2h$. The side walls are assumed to be rigid and the channel width is defined as w. As shown by Terrill,[16] imposing the condition $w/h \geq 8$ allows for the analysis to be simplified to two space dimensions. Additionally, the solution domain is reduced in size by assuming symmetry about the channel's midsection plane. The basic geometry is illustrated in Fig. 1 where a planar cross-section is shown; here, the mean-flow streamlines are calculated from Terrill's solution for large suction.[16] Under these auspices, the solution domain will be restricted to $0 \leq x^* \leq L$ and $0 \leq y^* \leq h$, where L is the channel length.

Under the influence of small variations in the suction rate, a channel that is closed at the head end and open at the aft end can develop longitudinal pressure oscillations of amplitude A. The corresponding frequency is specified by

$$\omega_s = (m - ½)\pi a_s / L \qquad (1)$$

where a_s refers to the stagnation speed of sound, and m is the oscillation mode shape number.

B. Limiting Conditions

In order to simplify the analysis, several limitations

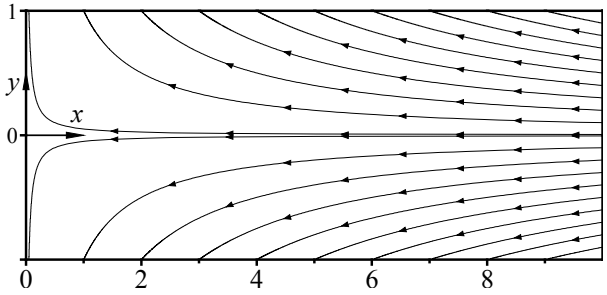

Fig. 1 System geometry showing streamlines calculated from Terrill's mean-flow solution for large suction in a channel.

must be observed. For example, we only consider a laminar and incompressible fluid. Also, A is taken to be small in comparison with then product of the stagnation pressure p_s and the ratio of specific heats γ. At the outset, the dimensionless wave parameter becomes $\bar{\varepsilon} \equiv A/(\gamma p_s) \ll 1$.

After variables are normalized, several non-dimensional parameters will appear in the governing equations. Included are the Mach number $M \equiv v_w / a_s$, the Strouhal number $S \equiv \omega_s h / v_w$, and the small perturbation parameter $\varepsilon \equiv 1/R = \nu/(v_w h)$. We will restrict our analysis to cases for which $M^2 < \bar{\varepsilon} < M < 1$. Furthermore, asymptotic results will be dependent on the condition $\varepsilon < 1$. Finally, a distinguished order between the Strouhal and Reynolds numbers will be later imposed. As suggested by Jankowski and Majdalani,[17] we have to posit $S \sim R$ to arrive at a uniformly valid WKB solution. We find this last condition to be the least restrictive since our asymptotic solutions appear to be applicable over a much broader range of Strouhal and suction Reynolds numbers than is prescribed by the distinguished order.

III. Problem Formulation

A. Flow Decomposition

Following the nomenclature used by Jankowski and Majdalani,[18] the governing equations are normalized and linearized. First, spatial coordinates, velocity, pressure, density, and time are normalized by letting

$$x = x^*/h\,,\ y = y^*/h\,,\ \boldsymbol{u} = \boldsymbol{u}^*/a_s \tag{2}$$

$$p = p^*/\gamma p_s\,,\ \rho = \rho^*/\rho_s\,, \text{ and } t = t^*\omega_s \tag{3}$$

where ρ_s is the stagnation density and asterisks denote dimensional variables. At the outset, the solution domain translates into $0 \le x \le l$ and $0 \le y \le 1$, where $l = L/h$ is the channel's dimensionless length. Second, density, pressure and velocity are perturbed in the pressure wave amplitude $\bar{\varepsilon}$. The result is

$$p(x,y,t) = p_0(x,y) + \bar{\varepsilon} p_1(x,y)\exp(-it) \tag{4}$$

$$\rho(x,y,t) = 1 + \bar{\varepsilon}\rho_1(x,y)\exp(-it) \tag{5}$$

$$\boldsymbol{u}(x,y,t) = M\boldsymbol{u}_0(x,y) + \bar{\varepsilon}\boldsymbol{u}_1(x,y)\exp(-it) \tag{6}$$

B. Leading Order Decomposition

After inserting Eqs. (2)–(6) into the governing equations, one collects terms of leading order in $\bar{\varepsilon}$; one finds

$$\nabla.\boldsymbol{u}_0 = 0 \tag{7}$$

$$M^2\left(\boldsymbol{u}_0.\nabla\right)\boldsymbol{u}_0 = -\nabla p_0 + M^2\varepsilon\left[4\nabla\left(\nabla.\boldsymbol{u}_0\right)/3 - \nabla\times\left(\nabla\times\boldsymbol{u}_0\right)\right] \tag{8}$$

Following Berman,[1] a steady stream function can be defined such that

$$\Psi = -xF(y) \tag{9}$$

This allows the velocity vector to be written as

$$\boldsymbol{u}_0 = u_0\hat{\boldsymbol{i}} + v_0\hat{\boldsymbol{j}} = (-xF', F) \tag{10}$$

The mean-flow momentum equation is then transformed into

$$F^{iv} + R\left(F'F'' - FF'''\right) = 0 \tag{11}$$

with $$F'(1) = F(0) = F''(0) = 0\,,\ F(1) = 1 \tag{12}$$

For the small suction case, Berman[1] has shown that the leading-order solution to Eq. (11) is

$$F(y) = \tfrac{1}{2}y(3-y^2) + \mathcal{O}(R/100); R < 20 \tag{13}$$

For the large suction case, Sellars[19] has found that $F(y) = y$. Sellars' result can also be extrapolated, in the limit as $R \to \infty$, from Terrill's higher-order approximation[16]

$$F(y) = \frac{R}{R-1}\left[y - \frac{1}{R}e^{-R(1-y)}\right] + \mathcal{O}(R^{-2})$$

$$= y + \mathcal{O}(R^{-1})\,,\ R \ge 20 \tag{14}$$

These examples can be used, whenever necessary, to illustrate the behavior of the conceptual function F.

C. Time Dependent Equations

By collecting terms of order $\bar{\varepsilon}$ in the governing equations, one obtains

$$-i\omega\rho_1 + \nabla\cdot\boldsymbol{u}_1 = -M\nabla\cdot\left(\rho_1\boldsymbol{u}_0\right) \tag{15}$$

$$-i\omega\boldsymbol{u}_1 = -M\left[\nabla\left(\boldsymbol{u}_0\cdot\boldsymbol{u}_1\right) - \boldsymbol{u}_1\times\left(\nabla\times\boldsymbol{u}_0\right) - \boldsymbol{u}_0\times\left(\nabla\times\boldsymbol{u}_1\right)\right] - \nabla p_1 + M\varepsilon\left[4\nabla\left(\nabla\cdot\boldsymbol{u}_1\right)/3 - \nabla\times\left(\nabla\times\boldsymbol{u}_1\right)\right] \tag{16}$$

To make headway, the temporal field is then decomposed into an acoustic, pressure-driven, irrotational wave, and a rotational, vorticity-driven, solenoidal wave. This is effectuated by letting

$$\boldsymbol{u}_1 = \hat{\boldsymbol{u}} + \tilde{\boldsymbol{u}} \tag{17}$$

where $\nabla\times\hat{\boldsymbol{u}} = 0$ and $\nabla\cdot\tilde{\boldsymbol{u}} = 0$.

After applying Eq. (17) to Eqs. (15)–(16) and solving for the acoustic axial velocity and pressure, one finds

$$\hat{p} = \cos(\omega x) + \mathcal{O}(M) \tag{18}$$

$$\hat{\boldsymbol{u}} = i\sin(\omega x)\,\hat{i} + \mathcal{O}(M) \tag{19}$$

where $\omega \equiv \omega_s h / a_s$ is the dimensionless wave frequency. Collecting terms describing the vortical set, and using Eq. (10), a solution for the axial rotational velocity is obtained through the use of separation of variables. By letting

$$\tilde{u} = X(x)\,Y(y) \tag{20}$$

the solution becomes

$$\tilde{u}(x,y) = -i\sum_{n=0}^{\infty} \frac{(-1)^n (\omega x)^{2n+1}}{(2n+1)!} Y_n(y) \tag{21}$$

Completing the solution requires finding Y_n from the following boundary value problem:

$$\varepsilon \frac{\mathrm{d}^2 Y_n}{\mathrm{d}y^2} - F\frac{\mathrm{d}Y_n}{\mathrm{d}y} + \left[iS + (2n+2)F'\right]Y_n = 0 \tag{22}$$

$$\text{with} \qquad Y_n(1) = 1 \text{ and } Y_n'(0) = 0 \tag{23}$$

where $S \equiv \omega / M$ is the Strouhal number.

IV. Multiple-Scales Analysis

A. The Relevant Scales

Equation (22) can be solved using a two-variable multiple-scales expansion provided the correct coordinate transformations are known. After several trials, we find that the unique set of scales that enables us to solve the problem consists of

$$y = y \text{ and } z = \frac{1-y}{\varepsilon} \tag{24}$$

Note that y is the outer scale, while z is the inner variable obtained by stretching the original coordinate near the wall. Therein, a boundary layer can be expected due to the form of Eq. (22).

B. Transformed Partial Differential Equations

Insertion of the inner scale into Eq. (22) gives

$$\frac{\mathrm{d}^2 Y_n}{\mathrm{d}z^2} + F\frac{\mathrm{d}Y_n}{\mathrm{d}z} + \left[iS + (2n+2)F'\right]\varepsilon Y_n = 0 \tag{25}$$

Assuming that Y_n is a function of both scales transforms the derivatives into

$$\frac{\mathrm{d}Y_n}{\mathrm{d}z} = \frac{\partial Y_n}{\partial z} - \varepsilon\frac{\partial Y_n}{\partial y} \tag{26}$$

$$\frac{\mathrm{d}^2 Y_n}{\mathrm{d}z^2} = \frac{\partial^2 Y_n}{\partial z^2} - 2\varepsilon\frac{\partial^2 Y_n}{\partial y \partial z} + \mathcal{O}\left(\varepsilon^2\right) \tag{27}$$

Now letting $Y_n = Y_0 + \varepsilon Y_1 + \mathcal{O}\left(\varepsilon^2\right)$, Eq. (25) becomes

$$\frac{\partial^2 Y_0}{\partial z^2} + \varepsilon\frac{\partial^2 Y_1}{\partial z^2} - 2\varepsilon\frac{\partial^2 Y_0}{\partial y \partial z} + F\frac{\partial Y_0}{\partial z} + \varepsilon F\frac{\partial Y_1}{\partial z}$$

$$-\varepsilon F\frac{\partial Y_0}{\partial y} + \varepsilon\left[iS + (2n+2)F'\right]\left(Y_0 + \varepsilon Y_1\right) = 0 \tag{28}$$

From Eq. (28), two equations can be segregated to determine Y_0 and Y_1 at leading and first orders. With the distinguished limit of $S \sim \varepsilon^{-1}$, the $\mathcal{O}(1)$ equation can be deduced to be

$$\frac{\partial^2 Y_0}{\partial z^2} + F\frac{\partial Y_0}{\partial z} + iS\varepsilon Y_0 = 0 \tag{29}$$

Similarly, the $\mathcal{O}(\varepsilon)$ terms give

$$\frac{\partial^2 Y_1}{\partial z^2} + F\frac{\partial Y_1}{\partial z} + iS\varepsilon Y_1$$

$$= 2\frac{\partial^2 Y_0}{\partial y \partial z} + F\frac{\partial Y_0}{\partial y} - (2n+2)F'Y_0 \tag{30}$$

C. The Basic Multiple-Scales Solution

Solving Eq. (29) yields

$$Y_0 = A_1(y)\exp\left[\left(\sqrt{F^2 - 4iS\varepsilon} - F\right)\frac{z}{2}\right]$$

$$+A_2(y)\exp\left[-\left(F + \sqrt{F^2 - 4iS\varepsilon}\right)\frac{z}{2}\right] \tag{31}$$

After differentiating Eq. (31) and evaluating the right hand side of Eq. (30), one finds that prevention of secular terms at $\mathcal{O}(\varepsilon)$ can be accomplished if, and only if,

$$\frac{\mathrm{d}A_1}{\mathrm{d}y} = \left[\frac{(4n+6)F'\sqrt{F^2 - 4iS\varepsilon} - 2FF'}{2\left(F^2 - 4iS\varepsilon\right)}\right]A_1 \tag{32}$$

$$\frac{\mathrm{d}A_2}{\mathrm{d}y} = \left[\frac{(4n+6)F'\sqrt{F^2 - 4iS\varepsilon} + 2FF'}{2\left(4iS\varepsilon - F^2\right)}\right]A_2 \tag{33}$$

where primes denote differentiation with respect to y. After integration, the solutions to Eqs. (32)–(33) can be substituted into Eq. (31). The result is

$$Y_0 = c_1\exp\left[I_1 + \left(\sqrt{F^2 - 4iS\varepsilon} - F\right)\frac{(1-y)}{2\varepsilon}\right]$$

$$+c_2\exp\left[I_2 - \left(F + \sqrt{F^2 - 4iS\varepsilon}\right)\frac{(1-y)}{2\varepsilon}\right] \tag{34}$$

where

$$I_1 = \int_1^y \left[\frac{(4n+6)F'\sqrt{F^2 - 4iS\varepsilon} - 2FF'}{2\left(F^2 - 4iS\varepsilon\right)}\right]\mathrm{d}\eta \tag{35}$$

$$I_2 = \int_1^y \left[\frac{(4n+6)F'\sqrt{F^2 - 4iS\varepsilon} + 2FF'}{2\left(4iS\varepsilon - F^2\right)}\right]\mathrm{d}\eta \tag{36}$$

and where η is a dummy variable used for integration. Note that c_1 and c_2 are pure constants that can be determined from the two boundary conditions. In fact, by applying the conditions $Y_0(1)=1$ and $Y_0'(0)=0$, one concludes that

$$c_1 = 0 \text{ and } c_2 = 1. \tag{37}$$

At this point, the generalized multiple-scales solution is fully realized. One finds

$$Y_n = \exp\left[I_2 - \left(F+\sqrt{F^2-4iS\varepsilon}\right)\frac{(1-y)}{2\varepsilon}\right] \tag{38}$$

It should be noted that Eq. (36) can be carefully rearranged and integrated in a manner to yield a closed-form solution for any function F. When this is done, the complete solution Y_n can be expressed as

$$Y_n = \left(\frac{1+\sqrt{1-4iS\varepsilon}}{F+\sqrt{F^2-4iS\varepsilon}}\right)^{2n+3}\left(\frac{1-4iS\varepsilon}{F^2-4iS\varepsilon}\right)^{\frac{1}{2}} \times\exp\left[\left(F+\sqrt{F^2-4iS\varepsilon}\right)\frac{(y-1)}{2\varepsilon}\right] \tag{39}$$

D. The Multiple-Scales Suction Velocity

By substituting Eq. (39) into Eq. (21), one gets

$$\tilde{u}(x,y) = -i\sum_{n=0}^{\infty}\frac{(-1)^n}{(2n+1)!}\left[\frac{\omega x\left(1+\sqrt{1-4iS\varepsilon}\right)}{F+\sqrt{F^2-4iS\varepsilon}}\right]^{2n+1} \times\left(\frac{1+\sqrt{1-4iS\varepsilon}}{F+\sqrt{F^2-4iS\varepsilon}}\right)^{2}\left(\frac{1-4iS\varepsilon}{F^2-4iS\varepsilon}\right)^{\frac{1}{2}} \times\exp\left[\left(F+\sqrt{F^2-4iS\varepsilon}\right)\frac{(y-1)}{2\varepsilon}\right] \tag{40}$$

At this juncture, one must identify the term inside the summation to be the MacLaurin series expansion of the sine function. This enables us to further reduce the rotational component of the axial velocity into

$$\tilde{u}(x,y) = -i\left(\frac{1-4iS\varepsilon}{F^2-4iS\varepsilon}\right)^{\frac{1}{2}}\left(\frac{1+\sqrt{1-4iS\varepsilon}}{F+\sqrt{F^2-4iS\varepsilon}}\right)^{2} \times\exp\left[\left(F+\sqrt{F^2-4iS\varepsilon}\right)\frac{(y-1)}{2\varepsilon}\right] \times\sin\left[\frac{\omega x\left(1+\sqrt{1-4iS\varepsilon}\right)}{F+\sqrt{F^2-4iS\varepsilon}}\right] \tag{41}$$

Finally, using Eq. (17) and Eq. (19) the oscillatory axial velocity becomes

$$u_1(x,y) = i\left\{\sin(\omega x) - \left(\frac{1+\sqrt{1-4iS\varepsilon}}{F+\sqrt{F^2-4iS\varepsilon}}\right)^{2} \times\left(\frac{1-4iS\varepsilon}{F^2-4iS\varepsilon}\right)^{\frac{1}{2}}\exp\left[\left(F+\sqrt{F^2-4iS\varepsilon}\right)\frac{(y-1)}{2\varepsilon}\right] \times\sin\left[\frac{\omega x\left(1+\sqrt{1-4iS\varepsilon}\right)}{F+\sqrt{F^2-4iS\varepsilon}}\right]\right\} \tag{42}$$

V. The WKB Formulation

A. The WKB Expansion

Equation (22) can also be solved using a standard WKB approximation. The WKB method assumes that the solution exhibits an exponential behavior that is consistent with a damped wave. The corresponding solution can be constructed from a linear combination of exponential functions of the type

$$Y_n \sim \exp\left[\frac{1}{\delta}\sum_{j=0}^{\infty}\delta^j Q_j\right] \tag{43}$$

whose derivatives exhibit the form

$$Y_n' \sim \left[\frac{1}{\delta}\sum_{j=0}^{\infty}\delta^j Q_j'\right]\exp\left[\frac{1}{\delta}\sum_{j=0}^{\infty}\delta^j Q_j\right] \tag{44}$$

$$Y_n'' \sim \left[\frac{1}{\delta^2}\left(\sum_{j=0}^{\infty}\delta^j Q_j'\right)^2 + \frac{1}{\delta}\sum_{j=0}^{\infty}\delta^j Q_j''\right]\exp\left[\frac{1}{\delta}\sum_{j=0}^{\infty}\delta^j Q_j\right] \tag{45}$$

B. The $\mathcal{O}(\varepsilon)$ Expansion

Substituting Eqs. (43)–(44) into Eq. (22) gives

$$\frac{\varepsilon}{\delta^2}\left(\sum_{j=0}^{\infty}\delta^j Q_j'\right)^2 + \frac{\varepsilon}{\delta}\sum_{j=0}^{\infty}\delta^j Q_j'' - \frac{F}{\delta}\sum_{j=0}^{\infty}\delta^j Q_j' + iS + (2n+2)F' = 0 \tag{46}$$

Expanding to Q_1 gives

$$\frac{\varepsilon}{\delta^2}Q_0'^2 + \frac{2\varepsilon}{\delta}Q_0'Q_1' + \varepsilon Q_1'^2 + \frac{\varepsilon}{\delta}Q_0'' + \varepsilon Q_1'' - \frac{F}{\delta}Q_0' - FQ_1' + iS + (2n+2)F' = 0 \tag{47}$$

For the distinguished limit $S \sim \varepsilon^{-1}$, δ can be determined so that dominant terms appear at the same order. In fact, balancing leading terms stemming from the three main parts of Eq. (22) yields $\delta = \varepsilon$. At the outset, Eq. (47) becomes

$$\frac{1}{\varepsilon}Q_0'^2 + 2Q_0'Q_1' + Q_0'' - \frac{F}{\varepsilon}Q_0' - FQ_1' + iS + (2n+2)F' + \mathcal{O}(\varepsilon) = 0 \tag{48}$$

C. The Eikonal Term

From Eq. (48), two defining equations can be deduced for Q_0 and Q_1. At $\mathcal{O}(1/\varepsilon)$, one gets the so-called eikonal equation[20]

$$Q_0'^2 - FQ_0' + iS\varepsilon = 0 \tag{49}$$

In like fashion, the transport equation appears at $\mathcal{O}(1)$. One finds

$$Q_1' = \frac{Q_0'' + (2n+2)F'}{\left(F - 2Q_0'\right)} \tag{50}$$

Solving Eq. (49) gives dual solutions representing left and right-traveling waves; these are

$$Q_0 = \frac{1}{2}\int_1^y \left(\pm\sqrt{F^2 - 4iS\varepsilon} + F\right)\mathrm{d}\eta \tag{51}$$

The leading-order WKB solution can then be constructed from the linear combination of the two possible solutions; one gets

$$Y_n = c_1 \exp\left[\frac{1}{2\varepsilon}\int_1^y \left(\sqrt{F^2 - 4iS\varepsilon} + F\right)\mathrm{d}\eta\right] + c_2 \exp\left[\frac{-1}{2\varepsilon}\int_1^y \left(\sqrt{F^2 - 4iS\varepsilon} - F\right)\mathrm{d}\eta\right] \tag{52}$$

where the integration constants must be determined from the problem's boundary conditions, namely, $Y_n(1) = 1$ and $Y_n'(0) = 0$. One concludes that $c_1 = 1$ and $c_2 = 0$; being zero, the left-traveling wave contribution is inconsequential. This result is physically plausible because the current analysis does not consider wave motion within the solid walls.

D. The Basic WKB Solution

At this point, solving at $\mathcal{O}(\varepsilon)$ can be accomplished by integrating the transport equation. One finds

$$Q_1 = -\int_1^y \frac{\left[Q_0'' + (2n+2)F'\right]}{\left(2Q_0' - F\right)}\mathrm{d}\eta \tag{53}$$

In order to evaluate Eq. (53), one must use the physically meaningful solution in Eq. (51) (i.e., the one representing the right-traveling wave into the fluid). Starting with

$$Q_0 = \frac{1}{2}\int_1^y \left(\sqrt{F^2 - 4iS\varepsilon} + F\right)\mathrm{d}\eta \tag{54}$$

Eq. (53) becomes

$$Q_1 = -\frac{1}{2}\int_1^y \left[\frac{(4n+5)F'}{\sqrt{F^2 - 4iS\varepsilon}} + \frac{FF'}{F^2 - 4iS\varepsilon}\right]\mathrm{d}\eta \tag{55}$$

The complete WKB solution can now be constructed by combining both eikonal and transport solutions. One finds

$$Y_n = \exp\left\{\frac{1}{2\varepsilon}\int_1^y \left(\sqrt{F^2 - 4iS\varepsilon} + F\right)\mathrm{d}\eta - \frac{1}{2}\int_1^y \left[\frac{(4n+5)F'}{\sqrt{F^2 - 4iS\varepsilon}} + \frac{FF'}{F^2 - 4iS\varepsilon}\right]\mathrm{d}\eta\right\} \tag{56}$$

Note that the second term in Eq. (56) has been rearranged in a form that is prone to direct integration. The solution that ensues is

$$Y_n = \exp\left[\frac{1}{2\varepsilon}\int_1^y \left(\sqrt{F^2 - 4iS\varepsilon} + F\right)\mathrm{d}\eta\right] \times \left(\frac{1 + \sqrt{1 - 4iS\varepsilon}}{F + \sqrt{F^2 - 4iS\varepsilon}}\right)^{2n+\frac{5}{2}} \left(\frac{1 - 4iS\varepsilon}{F^2 - 4iS\varepsilon}\right)^{\frac{1}{4}} \tag{57}$$

E. The WKB Suction Velocity

Using Eqs. (17), (19), (21), and (57), the axial velocity developed from the WKB approach becomes

$$u_1(x,y) = i\left\{\sin(\omega x) - \left(\frac{1 + \sqrt{1 - 4iS\varepsilon}}{F + \sqrt{F^2 - 4iS\varepsilon}}\right)^{\frac{3}{2}} \times \left(\frac{1 - 4iS\varepsilon}{F^2 - 4iS\varepsilon}\right)^{\frac{1}{4}} \exp\left[\frac{1}{2\varepsilon}\int_1^y \left(F + \sqrt{F^2 - 4iS\varepsilon}\right)\mathrm{d}\eta\right] \times \sin\left[\frac{\omega x\left(1 + \sqrt{1 - 4iS\varepsilon}\right)}{F + \sqrt{F^2 - 4iS\varepsilon}}\right]\right\} \tag{58}$$

Note that, unlike Eq. (42), the WKB result is quasi-analytical. In view of its exponential term, the WKB velocity cannot be integrated in general for any function F. For some mean-flow functions, numeric integration of the exponential term can become necessary.

VI. Discussion

A. Solution Verification

The multiple-scale and WKB velocities given by Eq. (42) and Eq. (58) can be compared to numerical solutions of Eqs. (21)–(23). For that purpose, the two characteristic functions given by Eqs. (13) and (14) are used to describe the behavior at small and large R. It should be noted that, for the large suction case, one may use Sellars' form,[19] $F = y$, to obtain fully closed-form asymptotic solutions and an exact solution for Eqs. (21)–(23). A numerical solution becomes confirmatory. For the small suction case, however, using Berman's solution,[1] $F = \frac{1}{2}y(3 - y^2)$, prevents an exact solution for Eqs. (22)–(23). A numerical benchmark becomes a necessity. In this study, the numerical algorithm is based on Butcher's fifth order Runge-Kutta method that was used previously by Majdalani.[5] To insure accuracy,

a small tolerance is retained with a maximum step size of $\Delta y = 1\times10^{-6}$.

Berman's cubic polynomial function[1] also precludes obtaining a closed-form WKB solution. As a result, the quasi-analytical WKB solution for small suction requires numerical integration of the exponential term in Eq. (58).

The exact oscillatory velocity obtained for infinite suction at the porous surfaces has been previously given by Jankowski and Majdalani.[18] Their result was

$$u_1(x,y) = i\left[\sin(\omega x) - \sum_{n=0}^{\infty}\frac{(-1)^n(\omega x)^{2n+1}}{(2n+1)!} \times\frac{\Phi\left(-n-1-\frac{1}{2}iS,\frac{1}{2};\frac{1}{2}Ry^2\right)}{\Phi\left(-n-1-\frac{1}{2}iS,\frac{1}{2};\frac{1}{2}R\right)}\right] \tag{59}$$

where $\Phi(a,b;z)$ is the confluent hypergeometric function known as the Kummer function.[21] In this study, Eq. (59) is used to check the validity of the numerical routine.

B. Error Analysis

Using the exact solution as a benchmark, the maximum absolute error E_n in each of the approximations is plotted in Fig. 2. Therein, both the multiple-scales and WKB solutions are systematically compared to the exact solution over a useful range of Reynolds and Strouhal numbers. Following Bosley,[22] the maximum absolute error is shown versus ε for fixed S. Plotting these curves on logarithmic scales allows for the order of the error to be displayed by the slope. As $\varepsilon\to0$, the graph indicates that both approximate solutions exhibit an error of $\mathcal{O}(\varepsilon)$. This is consistent with the truncation error in the asymptotic series that were obtained at $\mathcal{O}(\varepsilon)$.

It should be noted that, during the quest for a distinguished limit in the WKB sequence, the assumption of $S \sim R$ was made. Figure 2 shows that the accuracy of our solutions does not deteriorate when this condition is deviated from. In fact, both multiple-scales and WKB solutions appear to be increasingly more accurate as S is increased at constant ε, or as $\varepsilon\to0$ at constant S. The $S \sim R$ condition remains asymptotically true since the error approaches zero the fastest when both $S\to\infty$ and $R\to\infty$. We also note in Fig. 2 that the error in the multiple-scales result is smaller than that in the WKB. In both cases, the error appears to slightly increase at higher eigenvalues. Due to the increasingly more rapid wave damping that occurs at higher eigenvalues, the sensitivity of the error on the eigenvalue number n becomes immaterial. Contributions to the wave amplitude at higher n become less and less appreciable.

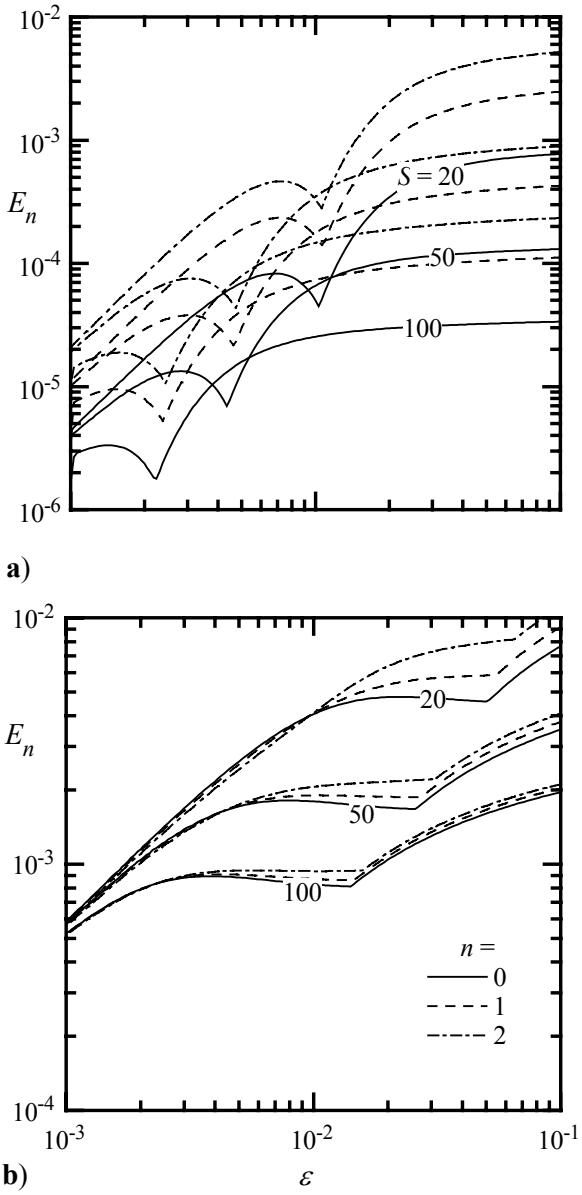

Fig. 2 The maximum absolute error between exact and asymptotic solutions shown over a range of physical attributes using a) multiple-scales and b) WKB.

C. Velocity Character

Figures 3–4 are used to illustrate the oscillatory suction velocity by plotting $u_1\exp(-it)$ at four equi-phased timelines and a range of operating parameters. In all figures, the profiles seem to agree favorably with the classic theory of laminar periodic flows.[23] Evidently, the velocity represents a spatially damped wave traveling in time. The wave exhibits a large inviscid core that stretches about the symmetry plane and a rotational boundary layer in the direct vicinity of

the wall. At the wall ($y = 1$), the no-slip condition is clearly satisfied. Above the wall, a small velocity overshoot of less than 10% of the inviscid amplitude is observed. This overshoot is of the same order as that reported in oscillatory flow experiments in tubes and annular regions bounded by hard walls.[24] The thickness of the rotational region is also comparable in size to the Stokes layer.[23]

In Fig. 3, both multiple-scales and WKB solutions are used to illustrate the effect of increasing the Reynolds number while keeping all other parameters constant. For the smallest suction level of $R = 10$, the relative effect of viscosity is the most appreciable. In this case, the rotational layer penetrates deeper into the channel than at higher Reynolds numbers. For the same physical reason, a relatively large overshoot is observed near the wall. As suction is increased, the relative importance of viscous effects becomes less significant. Profiles drawn at increasing Reynolds numbers show that the rotational layer undergoes a progressive compression, being pulled closer to the wall. With successive increases in suction, the companion overshoot diminishes as well. These physical characteristics can be explained in light of the asymptotic solutions that have been obtained. For example, from Eq. (42), it is possible to infer that the rotational amplitude must be strongly influenced by $\exp\left[-\frac{1}{2}R(1-y)\right]$. Thus, as the distance from the wall is increased, the wave amplitude decays more rapidly at larger R. Since the wave amplitude prescribes the boundary layer envelope, a shorter boundary layer follows. The overshoot is similarly affected since a smaller rotational contribution near the wall leads to a smaller total velocity.

The influence of the oscillation frequency is examined in Fig. 4 where the velocity is shown at small and large Strouhal numbers. Overall, it can be seen that an order of magnitude increase in frequency (for either small or large suction) causes a reduction in penetration depth and an augmentation in overshoot. This effect can be ascribed to the reduced spatial wavelength that, from Eq. (42), is inversely proportional to the Strouhal number. For larger S, the correspondingly shorter wavelength allows for the coupling between acoustic and rotational wave components to take place closer to the wall. Since the rotational velocity is larger near the wall, the vortical supplement is more appreciable when high frequency oscillations are present. When this supplemental contribution is added to the inviscid amplitude, a slightly larger overshoot is observed. The increased frequency also leads to faster particle reversals and, therefore, to more rapid viscous dissipation of the rotational disturbances born at the surface. This mechanism explains the reduced depth of penetration at higher frequencies.

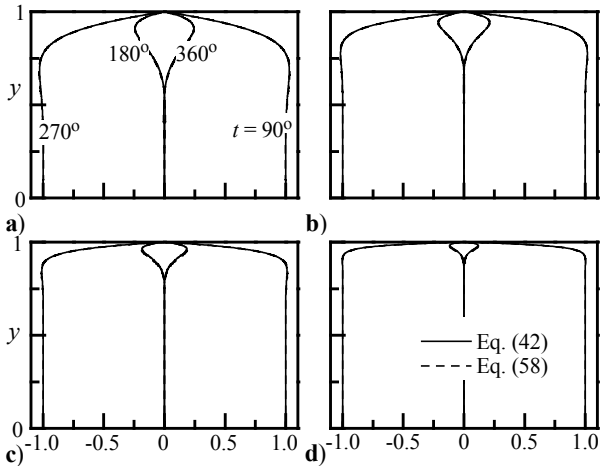

Fig. 3 The oscillatory axial velocity, $u_1\exp(-it)$, shown for $x/l = 1$, $m = 1$, and $S = 20$. Small suction profiles are shown for a) $R = 5$ and b) $R = 10$, while large suction profiles are shown for c) $R = 20$ and d) $R = 50$.

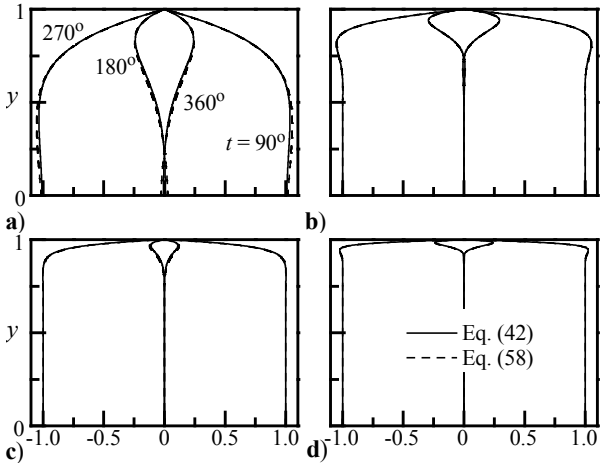

Fig. 4 The oscillatory axial velocity, $u_1\exp(-it)$, shown for $x/l = 1$ and $m = 1$. Parameters correspond to either a small $R = 3$ with a) $S = 10$ and b) $S = 100$ or to a large $R = 30$ with c) $S = 10$ and d) $S = 100$.

D. Comparison with the No-suction Case

The exact solution for zero wall suction has been developed for a one-dimensional flow in an infinitely long channel with hard walls and an oscillatory pressure triggered by 'pistons at infinity.' This can be extrapolated from Stokes' Second Problem. In our

nomenclature, the corresponding Stokes profile[23] can be written as

$$u_1 \exp(-it) = \sin(t) - \exp\left(-\sqrt{SR/2}y\right)\sin\left(t - \sqrt{SR/2}y\right). \quad (60)$$

Note that the Stokes' solution is independent of x; as such, it does not take into account the finite body length. In order to enable a reasonable comparison with our two-dimensional solutions, one must chose an axial location that exhibits a fixed spatial character that is indifferent to the oscillation mode shapes. The fixed pressure node at $x^* = L$ where $\omega x = \pi/2$ is found to be a suitable location that is unaffected by the length of the channel.

Another difficulty that must be overcome is the invalidity of our model at $v_w = 0$. Instead, a sufficiently small speed needs to chosen that will physically represent insignificant suction. An artificially negligible suction speed at the wall can be accomplished by equating v_w to Stokes' small diffusion speed. This condition can be realized by imposing

$$R = 2^{\frac{1}{3}} S. \quad (61)$$

Using $R = 10$ and $S = 7.94$ to satisfy Eq. (61), the indistinguishable multiple-scales and WKB solutions can now be compared to the Stokes profile in Fig. 5. Therein, one notes the fair resemblance of the hard wall solution and the asymptotic solutions developed for small suction. Unsurprisingly, the Stokes profile predicts a slightly larger rotational layer because fluid extortion in the small suction case attracts the shear layers closer to the surface.

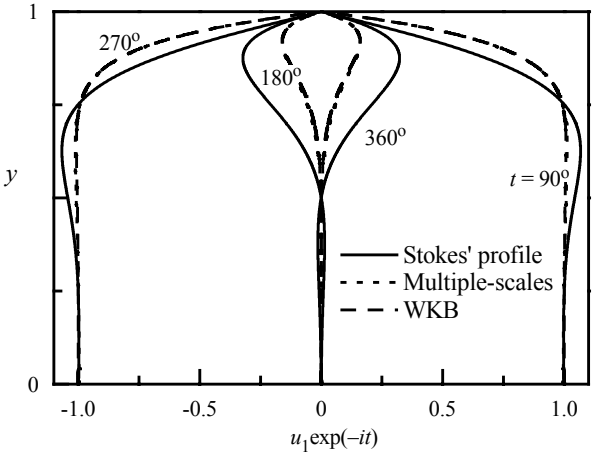

Fig. 5 Comparing the oscillatory velocity with and without suction (Stokes' profile) at four different times. Solutions are compared for $x/l = 1$, $m = 1$, $R = 10$ and $S = 8$.

VII. Concluding Remarks

This study provides two general asymptotic forms of the oscillatory suction flow in a porous channel. Both multiple-scales and WKB expansions coincide in predicting the form of the rapidly damped wave solutions that exist for both small and large suction cases. The solution type bears a striking resemblance to the Stokes profile in exhibiting small penetration depths and near-wall overshoot factors. Its advantage lies in its inclusion of two space dimensions that take into account the finite length of the channel. It can also account for different oscillation mode shapes and end-wall boundary conditions. For example, the current study is carried out for a closed-open channel configuration. The same can be extended, with some effort, to other geometric configurations. Another key realization in this study is the identification of the inner scale that can lead to a uniformly valid solution. The conventional presence of the boundary layer near the wall has enabled us to employ a linear magnification of the transverse coordinate. This linear distortion has provided the necessary resolution to achieve closure in a two-variable multi-scale expansion. Similar linear transformations of the independent variable were futile in the injection-driven flow analogue.[5,25] In the latter, nonlinear transformations and a generalized-scaling technique had to be applied in order to identify the underlying multi-scale structure. The injection-driven flow was also manageable by multiple-scales and WKB expansions.[5,25] In both cases, the multiple-scale solution proved to be more accurate despite its simplicity. In the current study, it has led to an unconditionally closed-form expression for an arbitrary mean flow function F. Its simplicity has also enabled us to understand or confirm the observed dependence on several operating parameters. In comparison to the injection-driven problem, the rotational effects are much smaller here. Suction seems to suppress the spreading of unsteady vorticity by convective removal at the wall. In both physical settings, increasing the frequency or Strouhal number leads to smaller penetration depths and larger overshoot factors. However, this cannot be said of the viscosity. In past studies concerned with injection,[5,25] higher viscosities have led to smaller depths of penetration. This was due to the wave decay being controlled by a key damping parameter, $\xi = \nu\omega^2 h / v_w^3$. At present, the damping role is usurped by the suction Reynolds number, $R = v_w h/\nu$. The reversal in the role of viscosity is clearly seen. Another dissimilarity lies in the size of the viscous layer. As confirmed by the distinguished limits demanded by the WKB formalism, the thickness of the inner layer decreases from $\delta = (-R)^{-\frac{1}{2}}$ for injection to $\delta = R^{-1}$ for suction. Thus, for the same physical properties and absolute

speed $|v_w|$, a smaller inner layer ensues during suction. More rapid changes in smaller distances are hence attributes of both mean and oscillatory components of suction-driven flows. This may explain the increased stiffness that has often prevented former investigations from exploring higher suction Reynolds numbers (cf. Yuan[26]). The increased stiffness with R requires progressively higher mesh resolutions during numerical integrations. In closing, it may be interesting to note that a simple sign switch in v_w has completely altered the problem and led to new asymptotic forms. We hope that the analytical framework presented here will be used in other studies involving time-dependent motions.

References

[1]Berman, A. S., "Laminar Flow in Channels with Porous Walls," *Journal of Applied Physics,* Vol. 24, No. 9, 1953, pp. 1232-1235.

[2]Zaturska, M. B., Drazin, P. G., and Banks, W. H. H., "On the Flow of a Viscous Fluid Driven Along a Channel by Suction at Porous Walls," *Fluid Dynamics Research,* Vol. 4, No. 3, 1988, pp. 151-178.

[3]Cox, S. M., "Two-Dimensional Flow of a Viscous Fluid in a Channel with Porous Walls," *Journal of Fluid Mechanics,* Vol. 227, 1991, pp. 1-33.

[4]Taylor, C. L., Banks, W. H. H., Zaturska, M. B., and Drazin, P. G., "Three-Dimensional Flow in a Porous Channel," *Quarterly Journal of Mechanics and Applied Mathematics,* Vol. 44, No. 1, 1991, pp. 105-133.

[5]Majdalani, J., "The Oscillatory Channel Flow with Arbitrary Wall Injection," *Journal of Applied Mathematics and Physics,* Vol. 52, No. 1, 2001, pp. 33-61.

[6]Catherall, D., Stewartson, K., and Williams, P. G., "Viscous Flow Past a Flat Plate with Uniform Injection," *Proceedings of the Royal Society, London, Series A,* Vol. 284, No. 1398, 1965, pp. 370-396.

[7]Proudman, I., "An Example of Steady Laminar Flow at Large Reynolds Number," *Journal of Fluid Mechanics,* Vol. 9, No. 4, 1960, pp. 593-612.

[8]Cole, J. D., and Aroesty, J., "The Blowhard Problem-Inviscid Flows with Surface Injection," *International Journal of Heat and Mass Transfer,* Vol. 11, No. 7, 1968, pp. 1167-1183.

[9]Terrill, R. M., "Laminar Flow in a Uniformly Porous Channel with Large Injection," *The Aeronautical Quarterly,* Vol. 16, 1965, pp. 323-332.

[10]Taylor, G. I., "Fluid Flow in Regions Bounded by Porous Surfaces," *Proceedings of the Royal Society, London, Series A,* Vol. 234, No. 1199, 1956, pp. 456-475.

[11]Berman, A. S., "Laminar Flow in an Annulus with Porous Walls," *Journal of Applied Physics,* Vol. 29, No. 1, 1958, pp. 71-75.

[12]Yuan, S. W., "Cooling by Protective Fluid Films," *Turbulent Flows and Heat Transfer,* Section G, Vol. V, edited by C. C. Lin, Princeton University Press, Princeton, New Jersey, 1959.

[13]Peng, Y., and Yuan, S. W., "Laminar Pipe Flow with Mass Transfer Cooling," *Journal of Heat Transfer,* Vol. 87, No. 2, 1965, pp. 252-258.

[14]Leadon, B. M., "The Status of Heat Transfer Control by Mass Transfer for Permanent Surface Structures," *Aerodynamically Heated Structures*, edited by P. E. Glaser, Prentice-Hall, Inc., Englewood Cliffs, New Jersey, 1962.

[15]Jaffrin, M. Y., and Shapiro, A. H., "Peristaltic Pumping," *Annual Review of Fluid Mechanics,* Vol. 3, 1971, pp. 13-36.

[16]Terrill, R. M., "Laminar Flow in a Uniformly Porous Channel," *The Aeronautical Quarterly,* Vol. 15, 1964, pp. 299-310.

[17]Jankowski, T. A., and Majdalani, J., "Imposition of Oscillatory Waves inside a Cylindrical Tube with Large Wall Suction," AIAA Paper 2001-2162, 28-30 May 2001.

[18]Jankowski, T. A., and Majdalani, J., "Acoustical and Vortical Interactions inside a Channel with Wall Suction," AIAA Paper 2000-1988, 12-14 June 2000.

[19]Sellars, J. R., "Laminar Flow in Channels with Porous Walls at High Suction Reynolds Numbers," *Journal of Applied Physics,* Vol. 26, No. 4, 1955, pp. 489-490.

[20]Bender, C. M., and Orszag, S. A., *Advanced Mathematical Methods for Scientists and Engineers*, McGraw-Hill Book Company Inc., New York, 1978.

[21]Abramowitz, M., and Stegun, I. A., *Handbook of Mathematical Functions*, National Bureau of Standards, New York, 1964.

[22]Bosley, D. L., "A Technique for the Numerical Verification of Asymptotic Expansions," *SIAM Review,* Vol. 38, No. 1, 1996, pp. 128-135.

[23]Rott, N., "Theory of Time-Dependent Laminar Flows," *High Speed Aerodynamics and Jet Propulsion –Theory of Laminar Flows,* Section D, Vol. IV, edited by F. K. Moore, Princeton University Press, Princeton, New Jersey, 1964, pp. 395-438.

[24]Richardson, E. G., "The Amplitude of Sound Waves in Resonators," *Proceedings of the Physical Society, London,* Vol. 40, No. 27, 1928, pp. 206-220.

[25]Majdalani, J., and Roh, T. S., "The Oscillatory Channel Flow with Large Wall Injection," *Proceedings of the Royal Society, Series A,* Vol. 456, No. 1999, 2000, pp. 1625-1657.

[26]Yuan, S. W., "Further Investigation of Laminar Flow in Channels with Porous Walls," *Journal of Applied Physics,* Vol. 27, No. 3, 1956, pp. 267-269.